International Forum on Aeroelasticity and Structural Dynamics
IFASD 2017
25-28 June 2017 Como, Italy

COMPUTATIONAL FLUID DYNAMICS BASED AEROELASTIC SYSTEM IDENTIFICATION AND FLUTTER PREDICTION

Matan Argaman[1] **and Daniella E. Raveh**[1]

[1]Faculty of Aerospace Engineering
Technion - Israel Institute of Technology
Haifa, Israel
margaman@campus.technion.ac.il
daniella@technion.ac.il

Keywords: Flutter prediction, Aeroelastic system identification,

Abstract: The paper presents a computational methodology for CFD-based flutter analysis that is based on system identification of the aeroelastic system at few sub-critical dynamic pressures. Autoregressive Exogenous (ARX) models of the aeroelastic system are estimated based on simulated aeroelastic modal responses to prescribed excitation of time-varying vertical velocities. A linear stability parameter of the system is computed for each dynamic pressure, and, by extrapolation, points to the flutter conditions. The method was demonstrated on three test cases of subsonic airfoil flutter (2 DOF plunge and pitch aeroelastic system), transonic airfoil flutter (2 DOF plunge and pitch aeroelastic system), and a generic transport aircraft at subsonic flow, with flutter mechanism involving three structural modes. In all cases the method resulted in accurate predication of the flutter point as compared to either full CFD aeroelastic simulation, or wind tunnel test results. The method is computationally efficient, as it only requires a single aeroelastic simulation, at two to three dynamic pressure values, to predict the flutter point (for each Mach number). The paper describes the methodology, and discusses the details of its application, its advantages, and shortcomings.

1 INTRODUCTION

Flutter analysis in the production environment is typically based on linear models, where the structure is modeled via a finite-element model, and the aerodynamics via a linear panel code. The main deficiency of linear panel codes is their inability to accurately estimate the unsteady aerodynamic forces, and, consequently, the flutter point, in the transonic regime.

Computational Fluid Dynamics (CFD) codes can accurately predict the flow field about complex realistic configurations in all flight regimes, and were used formerly for flutter analyses. Two approaches for CFD-based flutter analysis include the direct transient-response analysis, and the indirect approach that involves identification of reduced-order models (ROM) of the unsteady aerodynamics. In the direct approach, the flow and structural dynamics equations are coupled in time-marching aeroelastic simulation. Instabilities can be predicted by performing several such simulations, studying each transient for decaying or diverging response (e.g. 1, 2). Since aeroelastic simulations of realistic complex configurations require large computational resources, they cannot provide a viable methodology for production flutter analysis. The indirect approach looks for reduced-order models (ROMs), either linearized or nonlinear, for the

unsteady aerodynamics, which can then be coupled with the structural dynamics for transient response simulation, or can be used in stability analyses (e.g. 3–6).

The current study adopts concepts of aeroelastic system identification and flutter prediction from flight test methodologies, and applies them to CFD-based flutter analysis. In flutter flight tests, the dynamic characteristics of the aeroelastic system are interpreted from measured aircraft structural responses to external excitations, at sub-critical conditions (pre-flutter/LCO). Similarly, in the simulation environment, the aeroelastic system characteristics can be derived from simulated structural responses to some prescribed excitations, at pre-flutter conditions. In the simulation environment the focus is, naturally, on computational efficiency.

Over the years, several flutter flight testing methodologies were developed that rely on various excitation techniques, system identification and estimation methods, system stability parameters and flutter boundary prediction methods [7–15]. The Autoregressive Moving-Average (ARMA) method, originally suggested by Matsuzaki and Ando [9], uses system identification methods to fit an ARMA model that describes the aeroelastic system at sub-critical conditions. A linear stability parameter, computed from the ARMA model according to the Jury criterion, indicates the flutter/LCO onset. In flutter flight tests the advantage of the ARMA method is that the ARMA model coefficients are identified from structural responses to atmospheric turbulent excitations, without resorting to external excitation. This discrete-time method assumes the probabilistic distribution and frequency content of the excitation to be normally-distributed random white-noise, thus arguably suitable to describe natural air turbulence excitation. In the CFD-based simulation environment the equivalent of atmospheric turbulence excitation can be any prescribed excitation, with known deterministic and probabilistic characteristics. Thus, either an ARMA or an Autoregressive Exogenous (ARX) model can be fit to describe the aeroelastic system.

The ARMA method for flutter testing was originally developed for stationary measurements of a two-mode aeroelastic system. Later publications suggested extended versions of the method for non-stationary measurements [16], and multiple-mode systems [17], featuring advanced versions of the flutter stability parameter [18]. In CFD-based aeroelastic applications ARMA modeling was used to model the *unsteady aerodynamic forces* , which were then coupled with the structural dynamic system to predict flutter instability [6, 19]. The current study proposes a CFD-based flutter prediction approach that is based on ARMA modeling of the *aeroelastic* system, and the use of a linear stability parameter to predict the instability onset conditions.

The current paper presents the principals of ARMA/ARX system modeling, and the signal used for excitation. Several test cases demonstrate the application of the methodology for systems of various complexity, and at different flow conditions. Other than computational efficiency, another advantage of the proposed method is that it predicts the instability onset from sub-critical data, much like is done in flutter testing. Therefore it can be used in support of flutter flight tests, or even replacing some test points.

2 MATHEMATICAL MODEL

2.1 Dynamic Aeroelastic Model

Aeroelastic simulations are performed within the Elastic Zonal Navier-Stokes Solver (EZNSS) code. EZNSS is a second-order accurate dual time-stepping, implicit finite-difference code,

which is capable of analyzing the static and dynamic flow fields over a maneuvering elastic vehicle. The governing flow equations, turbulence models, and numerical methods are described in reference 20.

For the aeroelastic simulation, EZNSS solves the static or dynamic aeroelastic equation of motion (EOM) in modal coordinates:

$$[GM]\{\ddot{\xi}\} + [GC]\{\dot{\xi}\} + [GK]\{\xi\} = \{GF_A(t)\} \tag{1}$$

where $\{\xi\}$ is the vector of modal displacements, $[GM]$, $[GC]$, and $[GK]$ are the generalized mass, damping, and stiffness matrices, respectively, and $\{GF_A(t)\}$ is the generalized aerodynamic force vector. The latter is calculated as:

$$\{GF_A(t)\} = [\Phi_A]\{F_A(t)\} \tag{2}$$

where $\{F_A(t)\}$ is the vector of aerodynamic forces provided at the computational surface mesh, and $[\Phi_A]$ is the modal matrix, in which each column holds a structural elastic mode, mapped to the computational surface mesh. The generalized mass and stiffness matrices, and the modes matrix, are generated by a finite-element code and provided as inputs to the aeroelastic simulation. In the dynamic aeroelastic case, the aeroelastic EOM is solved for the generalized displacements following each CFD iteration. The time marching scheme for the dynamic aeroelastic EOM is provided in reference 20.

2.2 Dynamical System Representation in Discrete Time

Considering a viscously damped, linear, dynamic system of N degrees of freedom (DOF), the system oscillatory motion in the continuous time-domain is given by:

$$Y(t) = \sum_{n=1}^{N} [\hat{A}_n e^{s_n t} + \hat{B}_n e^{\overline{s}_n t}] \tag{3}$$

$$s_n = (-\zeta_n + i\sqrt{1-\zeta_n^2})\omega_n \tag{4}$$

where s is the complex Laplace parameter, $\overline{s}$ is the complex conjugate of s, $\hat{A}_n, \hat{B}_n$ are constants and ζ_n, ω_n are the system's n-th modal damping ratio and frequency parameters, respectively. For $\zeta_n \ll 1$, the system modal parameters can be extracted directly from s by:

$$s = (-\zeta_n + i)\omega_n \tag{5}$$

$$\omega_n = Im(s_n); \qquad \zeta_n = -\frac{Re(s_n)}{Im(s_n)} \tag{6}$$

Assuming that the system response Y(t) is sampled at a constant interval Δt, $y_i = Y(i\Delta t)$ is the response time series value at sample i with $i = 1..K$. The z complex frequency domain is commonly known as the discrete equivalent of the laplace domain. The z-transform [21] is defined by:

$$\tilde{Y}(z) = \sum_{n=0}^{\infty} y_n z^{-n} \qquad z = e^{s\Delta t} \tag{7}$$

Substituting equation 5 into 7, we obtain the z-plane roots as functions of the modal parameters:

$$z_n = e^{s_n \Delta t} = e^{-\omega_n \zeta_n \Delta t}[\cos(\omega_n \Delta t) + i \sin(\omega_n \Delta t)] \tag{8}$$

$$|z_n| = e^{-\omega_n \zeta_n \Delta t} \qquad \angle z_n = \omega_n \Delta t \tag{9}$$

Alternatively, the modal parameters may be expressed as a function of the z-plane roots by:

$$\omega_n = \frac{|\ln z_n|}{\Delta t} \qquad \zeta_n = -\frac{\ln |z_n|}{|\ln z_n|} \tag{10}$$

2.3 ARMA/ARX Model

For modeling purposes, the aeroelastic system is that of equations 1 and 2, including the flow parameters (Mach, dynamic pressure, angle of attack, etc.), and selection of CFD numerical parameters (mesh, turbulence model, scheme, time step, etc.). Figure 1 shows the aeroelastic system with the input of atmospheric turbulence (vertical gust velocities) and output of modal displacements.

Figure 1: Aeroelastic System

The ARMA model relates the modal displacements to the atmospheric turbulence excitation at the current and previous time steps and to previous time-step values of the modal displacements. Assuming any random excitation, the ARMA(p,q) model of the aeroelastic system is given by:

$$y_i + \phi_1 y_{i-1} + \phi_2 y_{i-2} + \ldots + \phi_p y_{i-p} = \epsilon_i + \theta_1 \epsilon_{i-1} + \theta_2 \epsilon_{i-2} + \ldots + \theta_q \epsilon_{i-q} \tag{11}$$

where p,q and ϕ_i, θ_i are the Autoregressive (AR) and Moving-average (MA) model orders and constants, respectively. ϵ_i is a time series that represents the normally distributed, white-noise, random sequence with zero mean and an unknown variance of σ^2. In summation notation, equation 11 may be rewritten as:

$$\sum_{n=0}^{p} \phi_n y_{i-n} = \sum_{m=0}^{q} \theta_m \epsilon_{i-m} \tag{12}$$
$$\theta_0 = \phi_0 = 1$$

The AR model order p is directly associated with the system order in the Laplace domain, thus for a system with N DOF, the AR order is taken as $p = 2N$. In order to represent aerodynamic lags, various AR orders, of $p > 2N$, are tested as well. The MA order q is typically taken as

$q = p - 1$, however the effect of MA order on the model accuracy is studied by using various MA orders of $q > p - 1$. The optimal combination of ARMA orders, p,q, can be chosen by using Akaike's information criterion (AIC). The combination of p and q which minimized the AIC are the most desirable.

$$AIC = -2log[\hat{L}] + 2(p + q + 1) \tag{13}$$

Where $\hat{L}$ is the maximum likelihood function of the ARMA model.

Applying the z-transform to equation 12, we obtain:

$$\sum_{n=0}^{p} \phi_n z^{-n} \sum_{n=0}^{\infty} y_n z^{-n} = \sum_{m=0}^{q} \theta_m z^{-m} \sum_{m=0}^{\infty} \epsilon_m z^{-m} \tag{14}$$

using equations 14 and 7, the system transfer function can be written in the z-plane as:

$$\tilde{H}(z) = \frac{\tilde{Y}(z)}{\tilde{\Upsilon}(z)} = \frac{\sum_{m=0}^{q} \theta_m z^{-m}}{\sum_{n=0}^{p} \phi_n z^{-n}} \tag{15}$$

from which the characteristic equation may be identified as:

$$G(z) = z^p \sum_{n=0}^{p} \phi_n z^{-n} = z^p + \phi_1 z^{p-1} + \phi_2 z^{p-2} + \ldots + \phi_p \tag{16}$$

$$G(z) = A_p z^p + A_{p-1} z^{p-1} + A_{p-2} z^{p-2} + \ldots + A_0 \tag{17}$$

$$A_j = \phi_{p-j}$$

According to Jury's stability criterion [21], the system is stable if and only if all roots of equation 16 are inside the unit circle, or, alternatively, if the following conditions are satisfied:

$$G(1) = A_p + A_{p-1} + \ldots + A_1 + A_0 > 0 \tag{18}$$

$$G(-1) = A_p - A_{p-1} + \ldots - A_1 + A_0 > 0 \tag{19}$$

$$F^+(k) = det(\hat{X}_k + \hat{Y}_k) > 0 \qquad (k = 1, 3, ..., p - 1) \tag{20}$$

$$F^-(k) = det(\hat{X}_k - \hat{Y}_k) > 0 \qquad (k = 1, 3, ..., p - 1) \tag{21}$$

$$\hat{X}_k = \begin{pmatrix} A_p & \ldots & A_{p-k+1} \\ 0 & \ddots & \vdots \\ 0 & 0 & A_p \end{pmatrix} \qquad \hat{Y}_k = \begin{pmatrix} A_{k-1} & \ldots & A_0 \\ \vdots & \ddots & 0 \\ A_0 & 0 & 0 \end{pmatrix} \tag{22}$$

Of these criteria, the $F^-(p-1)$ parameter is found to be the most critical, since it becomes negative as any of the system's roots crosses the unit circle, as derived in Ref. 22:

$$F^-(p-1) = A_p^{p-1} \prod_{i<j} (1 - z_i z_j) \tag{23}$$

where z_i, z_j are the two system's roots. Torii and Matsuzaki [18] have suggested the following stability parameter formulation for a 2-DOF aeroelastic systems (binary flutter mechanism):

$$F_Z = \frac{F^-(p-1)}{F^-(1)^2} = \frac{F^-(p-1)}{(A_p - A_0)^2} \tag{24}$$

This parameter was shown to vary as a linear function of the dynamic pressure, thus offering a convenient indication of the instability onset. While it was demonstrated for 2-DOF aeroelastic system, this formulation fits for higher degrees of freedom as well, by choosing the desired AR order.

2.3.1 ARX/ARMAX Models

Similarly to the ARMA model development, a more general model that depends on an exogenous known signal source may be identified as the following ARMAX(p, q, m) model:

$$y_i + \phi_1 y_{i-1} + \ldots + \phi_p y_{i-p} = \epsilon_i + \theta_1 \epsilon_{i-1} + \ldots + \theta_q \epsilon_{i-q} + \eta_1 u_i + \eta_2 u_{i-1} + \ldots + \eta_{m+1} u_{i-m} \tag{25}$$

where u_i is the exogenous signal and η_i are its corresponding coefficients. Removing the MA part from ARMAX results in the following ARX(p, m) model:

$$y_i + \phi_1 y_{i-1} + \ldots + \phi_p y_{i-p} = \eta_1 u_i + \eta_2 u_{i-1} + \ldots + \eta_{m+1} u_{i-m} \tag{26}$$

In the simulation environment the excitation signal is known, thus an ARX (rather than an ARMA) model can be identified, and should provide a more accurate model of the system. The advantage of ARMA model is that it follows flutter flight test procedures, and thus can be used in support of such tests. For both ARMAX and ARX models, eqs. 16 to 24 still hold, as the characteristic equation depends solely on the AR coefficients. In the current study, the ARX model coefficients, ϕ_i, η_i, are computed using the MATLAB System Identification Toolbox ARX function.

2.4 Excitation Signal

System identification is based on modal responses to time-varying vertical (heave) velocities. The gust velocity is a filtered random time series with Gaussian distribution, in which filtering is applied to control the range of excited frequencies, such that any frequency spectrum of interest can be excited. The excitation is introduced to the flow field by prescribing a vertical velocity to all the grid points, as described in reference 23. For three-dimensional aircraft cases the vertical velocity is assumed constant along the span.

3 TEST CASES

3.1 2D Wing Section - NACA0012

The first test case is that of a spring-suspended NACA 0012 airfoil section, at incompressible flow. It is the same test case used by Matsuzaki and Torii [24], and serves for method validation. Figure 2 shows the aeroelastic model. Model parameters are half-chord, $b = 0.5$, elastic axis at $a = -0.4$, static unbalance, $x_\alpha = 0.4$, radius of gyration, $r_\alpha = 0.5$, mass ratio, $\mu = 40$, and uncoupled frequencies, $\omega_h = 50\ rad/s$, and $\omega_\alpha = 100\ rad/s$. These translate to coupled frequencies of $\omega_1 = 49\ rad/s$ ($f_1 = 7.7\ Hz$), and $\omega_2 = 112\ rad/s$ ($f_2 = 17.7\ Hz$). Figure 3 shows an ω-V-g plot computed using linear Theodorsen aerodynamics. Flutter onset is at $V_f = 145m/s$, and dynamic pressure of $Q_f = 12878Pa$. These values serve as initial guess of the flutter point.

ARMA models of the aeroelastic system were identified at four dynamic pressure values, ranging from 0.67 to 0.97 of Q_f, the initial guess of the flutter onset. At each dynamic pressure, an ARX model was identified based on simulated responses of the two modal DOFs to an excitation signal. Responses were simulated by time-marching the aeroelastic EOM (Eq. 1), at Mach number of 0.35, and varying altitudes.

The excitation signal is time-varying, randomly distributed vertical velocity, filtered above $120/Hz$. The max amplitude, w_g, was set to equivalent angle of attack of 1° ($w_g/V_\infty = 1^\circ$). In general, the amplitude of the excitation signal should be large enough to excite the system, and provide good data coherence for system identification, but it should not be too large to trigger nonlinear responses. The amplitude of the excitation signal is also directly linked to the simulation run time, since large excitations require a larger number of sub-iterations between each two consecutive time steps for the flow field to converge properly.

Aeroelastic responses were simulated based on the inviscid, Euler equations. The computational mesh is of C-O, type with dimensions of 301x145 in the chordwise, and perpendicular directions, respectively. The time-step of the simulation was set to $dt = 10^{-3}\ s$, and the simulation was preformed over $N = 50000$ time steps.

When generating identification data from CFD simulations, the sampling rate equals the reciprocal of the simulation time step, $f_s = 1/dt$, from which signals of frequencies up to half the sampling rate can be reconstructed (denoted by the Nyquist frequency, f_{Nyq}). Because typical CFD time steps are small, due to scheme convergence limitations, f_{Nyq} is typically high, and exceeds the frequency range of interest for aeroelastic problems. The simulation length, that is, the number of time steps simulated N, determines the frequency resolution, f_{Nyq}/N, which should be adequate for representing the lowest frequency of interest in the aeroelastic system. Therefore, the simulation time step and length should be adjusted to fit the desired frequency range and resolution. In the current test case $f_{Nyq} = 500Hz$, and the frequency resolution is 0.01 Hz.

Figure 4 shows the Power Spectral Density (PSD) function of the first and second mode responses, ξ_1, and ξ_2, computed at two dynamic pressure values of $0.67Q_f$ and $0.97Q_f$. PSDs were computed using Welch's averaged modified periodogram method, with eight windows, and 50% overlap. At both dynamic pressure values the modal responses capture the system's aeroelastic frequencies.

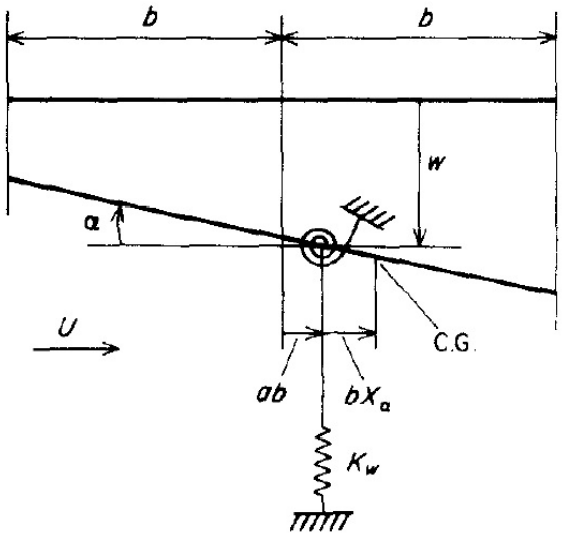

Figure 2: Aeroelastic Model of NACA0012 wing section

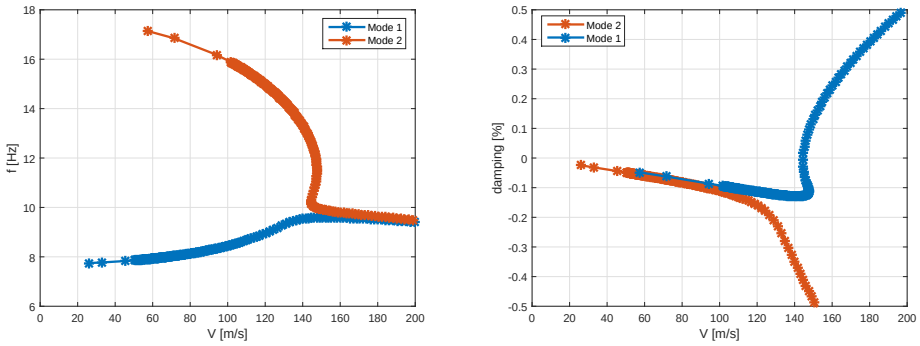

(a) Frequency vs. Velocity (b) Damping vs. Velocity

Figure 3: Linear Flutter Analysis of NACA0012 wing section

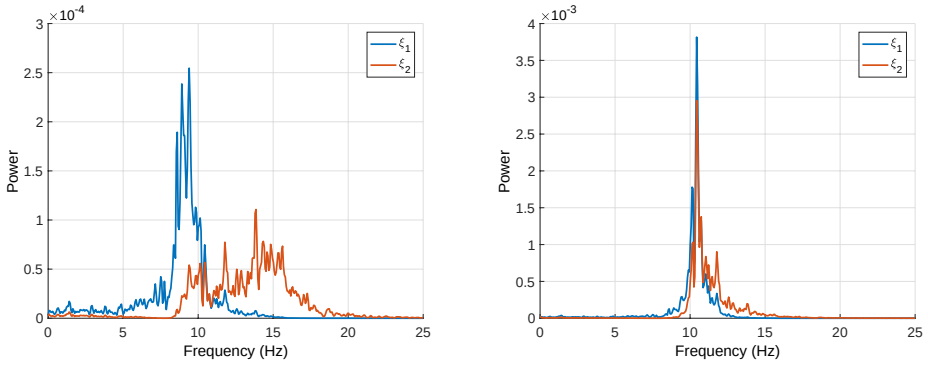

(a) $0.67Q_f$ (b) $0.97Q_f$

Figure 4: PSD of the modal responses at $0.67Q_f$,and $0.97Q_f$, NACA0012 wing section

ARX models of the aeroelastic system were identified based on the ξ_1 simulated response, at dynamic pressure values of $0.67Q_f$, $0.9Q_f$, $0.95Q_f$ and $0.97Q_f$. Since this model has only two degrees of freedom, the AR order was set to $p = 4$ (two modes and their conjugates), and the MA order was set to $q = 5$.

Figure 5 shows the roots of the characteristic equation of the identified aeroelastic system, over the unit circle. The unstable modes shift towards the edge of the unit circle as the dynamic pressure approaches that of flutter. Figure 6 shows the aeroelastic frequencies and damping coefficients, calculated from the ARX models' roots (Eq. 10).

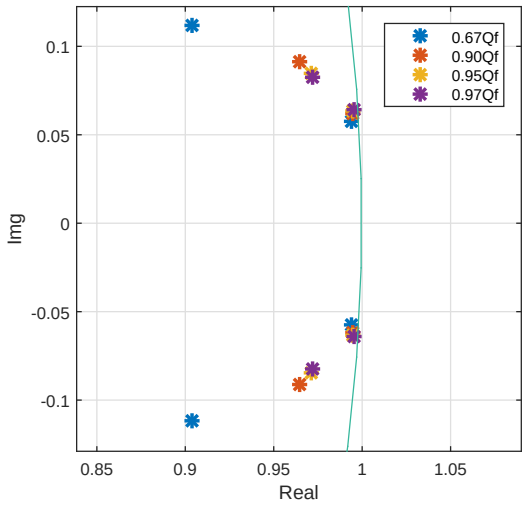

Figure 5: Roots of ARX models, p=4, q=5, NACA0012 wing section

Figure 7 shows the stability parameter values, calculated based on the identified ARX models (Eq. 24). A linear trend line based on stability parameter values at dynamic pressures of $0.9 - 0.97Q_f$ predicts the flutter point at $1.026Q_f$, while a trend line based on the two higher dynamic pressures values only ($0.95Q_f$ and $0.97Q_f$) predicts flutter at $1.038Q_f$. The stability parameter at $0.67Q_f$ does not follow these linear trends, indicating that flutter prediction should

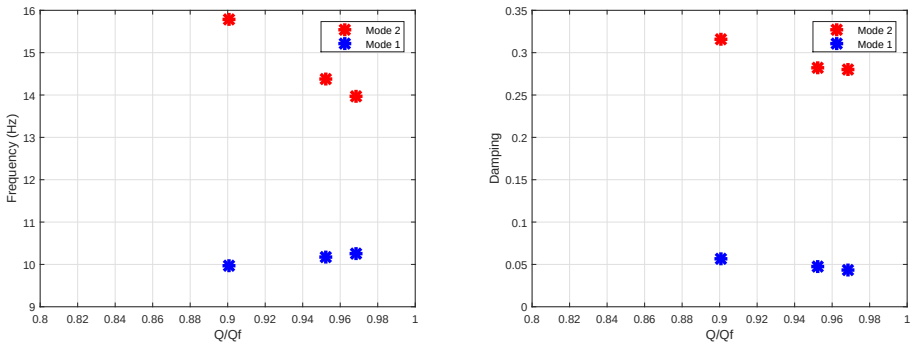

(a) Modal Frequencies (b) Modal Damping

Figure 6: Modal frequencies and Damping of ARX models, p=4, q=5, NACA0012 wing section

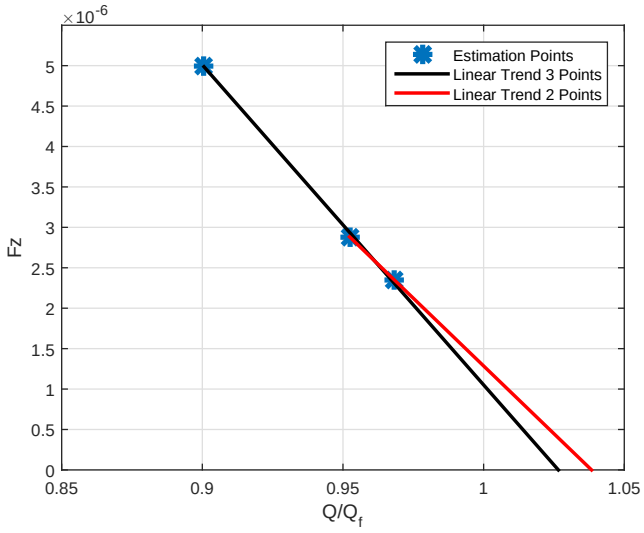

Figure 7: Stability Parameter of NACA0012 wing section

be performed based on data at dynamic pressure values that are close to the flutter point.

Figure 8 shows the sensitivity of the stability parameter to the sample data size. Stability parameter values converge for $N = 5000$ and above, indicating that, at least for this test case, the method only requires simulations as short as 5000 time steps at each dynamic pressure in order to provide a good prediction of the flutter onset.

The flutter prediction process is wrapped-up by running an aeroelastic simulation at the predicted flutter dynamic pressure. At dynamic pressure of $1.038Q_f$ the system is exactly on the verge of instability (Figure 9(a)), while at $1.026Q_f$ the responses are decaying (Figure 9(b)). The small discrepancy (1.17%) in the predicted flutter point based on the three-point linear trend is not surprising, considering the fact that this is a case of hard flutter, in which very small changes in the dynamic pressure are associated with large differences in the system's stability. In such cases an exact flutter point can be obtained only when based on responses very close to flutter.

3.2 Benchmark Super Critical Wing (BSCW) Configuration

The BSCW is a rigid, semispan, rectangular wing, with a chord of 0.4064 m (16 inches), a span of 0.8128 m (32 inches), and a SC(2)0414 supersonic airfoil. The BSCW configuration was tested for flutter in the NASA Langley Transonic Dynamics Tunnel, where the rigid wing was suspended from a pitch and plunge apparatus, simulating two degrees-of-freedom flutter. [25] Table 1 presents the frequencies, stiffness, and inertia properties of the model.

	Frequency (Hz)	Generalized Stiffness (Nm)	Generalized Mass (kgm^2)
Plunge	3.3	437.7	1.0
Pitch	5.2	1067.3	1.0

Table 1: BSCW structural modal properties

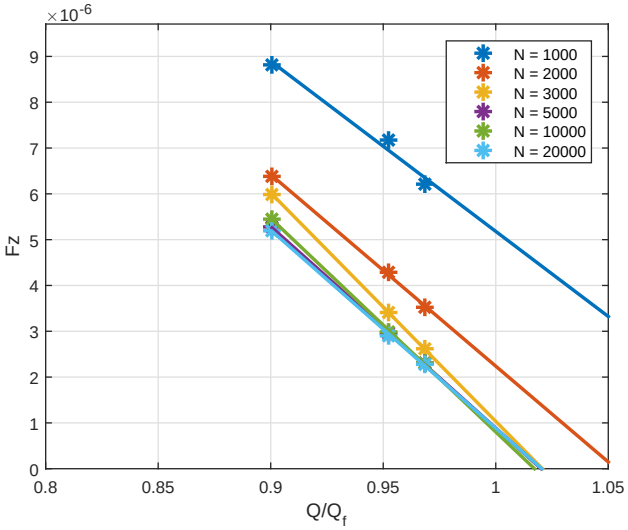

Figure 8: Stability parameter sensitivity to the estimation data length, N, NACA0012 wing section

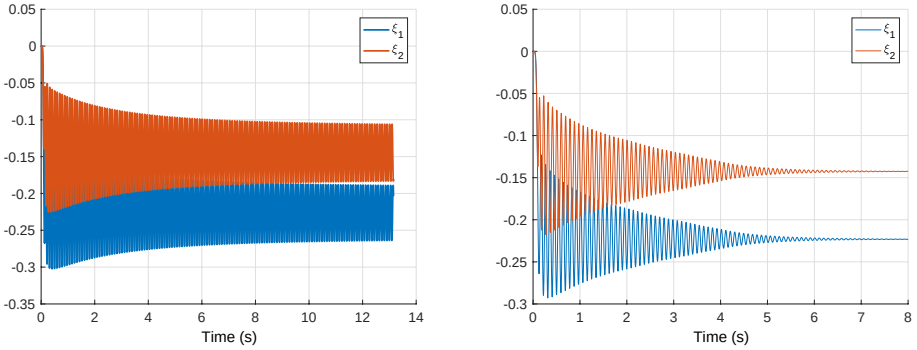

(a) $1.038Q_f$ (b) $1.026Q_f$

Figure 9: Modal responses at the predicted flutter point (a) and at a lower dynamic pressure (b), NACA0012 wing section

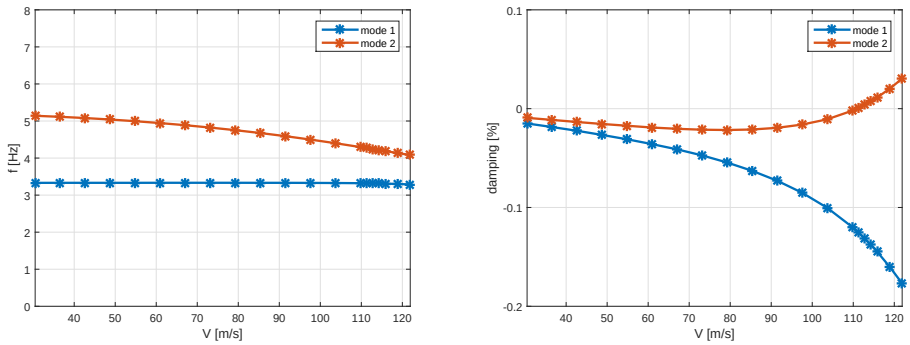

(a) Frequency vs. Velocity (b) Damping vs. Velocity

Figure 10: Linear flutter analysis of the BSCW, Mach 0.74

The wing was tested for flutter in air and in R-12 gas, at various flow conditions. The BSCW configuration was recently used for the Aeroelastic Prediction Workshop. [26] Reference data included experimental results in R-12 gas, at Mach 0.74, 0°angle of attack. At these conditions flutter was encountered at dynamic pressure of $8092\ Pa$, at a frequency of $4.3\ Hz$.

Figure 10 shows $\omega - V - g$ plot computed for this case with a linear panel model, using the ZAERO software [1]. The computed flutter speed is $111\ m/s$, corresponding to dynamic pressure of $Qf = 7476\ Pa$, and the flutter frequency is $4.3\ Hz$. The linear solution serves as an initial guess of the flutter point.

CFD simulations were computed on a C-O type mesh with dimensions of 253x71x99 in the chordwise, spanwise, and perpendicular directions, respectively. All simulations are based on the viscous Navier-Stokes equations, using the Spalart-Allmaras turbulence model. Details of the computational parameters can be found in Raveh et al. [20]. Aeroelastic simulation at the wind-tunnel test flutter dynamic pressure of $8092\ Pa$ yielded slightly diverging responses, at a frequency of $4.4\ Hz$. The exact flutter point was not pinpointed in the aeroelastic simulation, hence there is no exact reference for the flutter dynamic pressure.

An ARX model was identified at four dynamic pressure values, ranging from 0.8 to 1.03 Q_f. At each dynamic pressure, an ARX model was identified based on simulated responses of the plunge DOF to an excitation signal of vertical velocity, with equivalent amplitude of $4°$ angle of attack. To ensure sufficient observability in the estimation process, the excitation signal was filtered above $30\ Hz$. The CFD simulation time step was $dt = 10^{-3}\ s$, for which the frequencies up to $f_{Nyq} = 500\ Hz$ can be identified. The simulations were performed over 4000-5000 time steps (frequency resolution of 0.125 and 0.1 Hz, respectively), which are required for sufficiently converged estimation of the stability parameter.

The AR order of the ARX model used was $p = 6$ - four roots for the number of modes (and their conjugates), and two for aerodynamic legs, which were required in this case. An AR order of $p = 4$ resulted in two complex and two real roots, thus indicating that a higher order model is required. MA orders of $q = 7$ to $q = 11$ yielded best flutter prediction results (when compared to the wind tunnel dynamic pressure), while the Fz parameter estimation only converged at high MA orders of $q = 25$ and above. Figures 11 shows the estimation sensitivity to the MA order.

[1] www.zonatech.com/ZAERO.htm

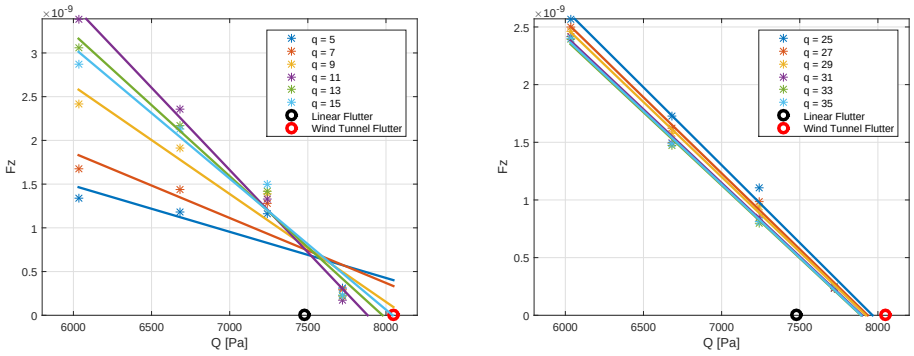

(a) Sensitivity MA order 5 to 15 (b) Sensitivity MA order 25 to 35

Figure 11: Stability parameter sensitivity to the MA order, BSCW

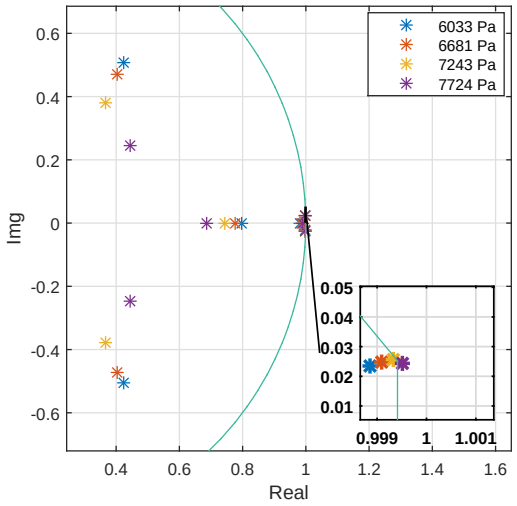

Figure 12: Roots of ARMA models, $p = 6$, $q = 25$, BSCW

As can be seen, this case requires more input history information (higher order of MA) in order to obtain well-converged stability parameter estimation.

Figure 12 shows the roots of the characteristic equation for each ARX model, over the unit circle. The roots are seen to shift towards the edge of the unit circle with increasing dynamic pressure. As expected, there are two complex roots for the aeroelastic modes, and two real roots for the aerodynamic legs. Figure 13 shows stability parameter estimation for MA order of 25, based on data set of $N = 4000$ points. A linear trend line predicts flutter at $1.065Q_f = 7962\ Pa$. This value is 0.98 of the wind tunnel flutter dynamic pressure. It was not yet verified by a full aeroelastic CFD simulation.

3.3 Generic Transport Aircraft

The third test case involves a generic transport aircraft shown in figure 14. The geometrical properties of the model are described in reference 27. Figure 15 shows the modes that were included in the flutter analysis, with their frequencies.

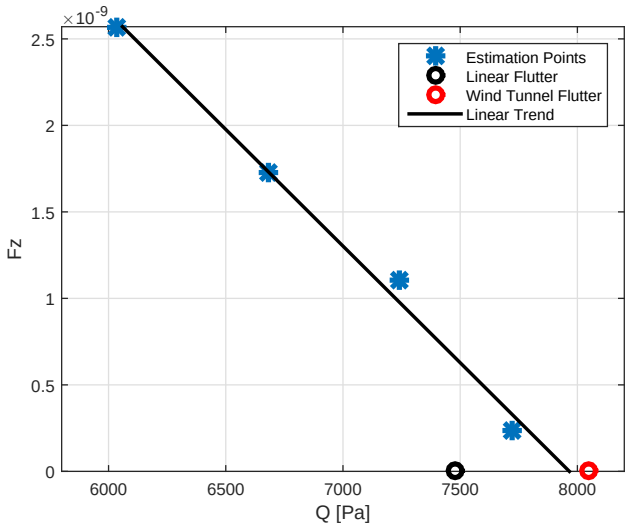

Figure 13: Stability parameter of the BSCW, $p = 6$, $q = 25$

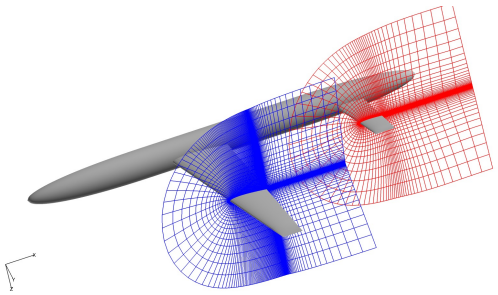

(a) geometry and mesh

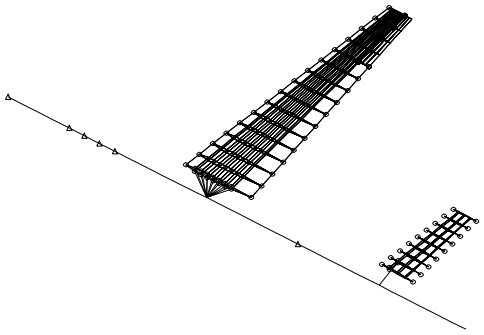

(b) finite-element model

Figure 14: Generic Transport Aircraft model

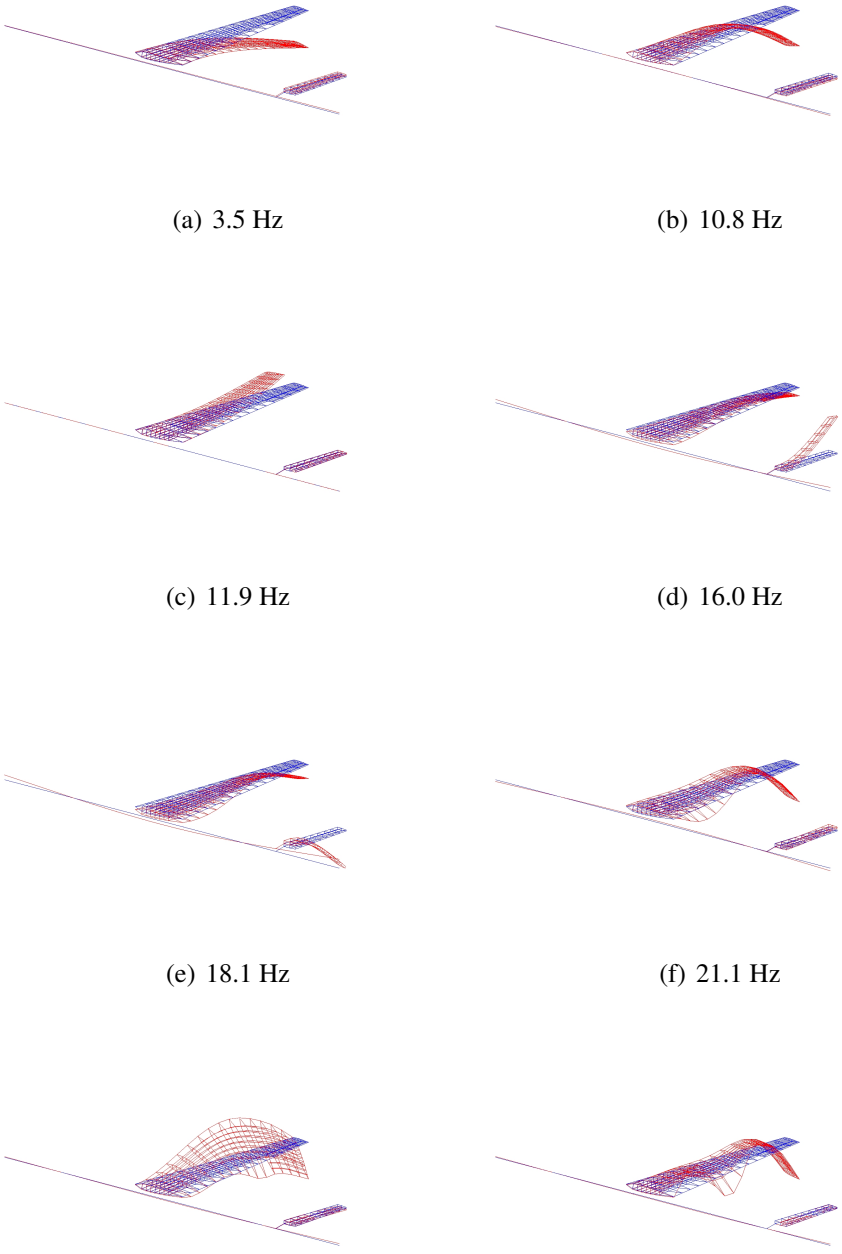

(a) 3.5 Hz (b) 10.8 Hz

(c) 11.9 Hz (d) 16.0 Hz

(e) 18.1 Hz (f) 21.1 Hz

(g) 22.5 Hz (h) 29.9 Hz

Figure 15: Modes of the Generic Transport Aircraft

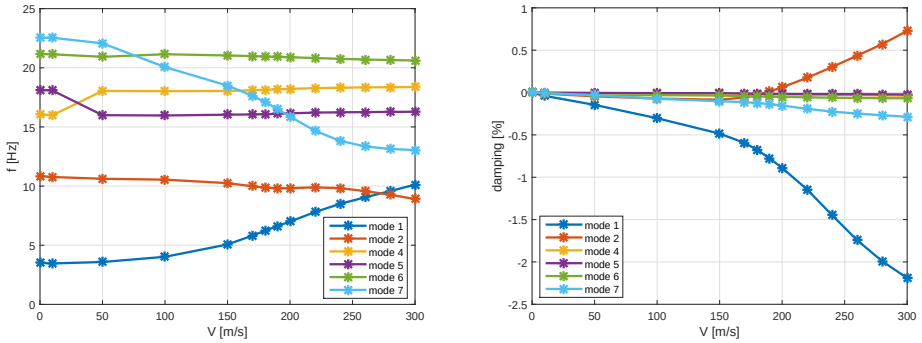

(a) Frequency vs. Velocity (b) Damping vs. Velocity

Figure 16: Linear flutter analysis, Mach=0.53, Generic Transport Aircraft

Flutter was computed at the subsonic regime, Mach 0.53, with three rigid body modes and eight elastic modes. Similarly to other two cases, linear flutter analysis, using ZAERO, was performed in order to assess the flutter velocity and mechanism. $\omega - V - g$ plot (Figure 16) shows flutter of the second elastic mode, at velocity of 179 m/sec, and frequency of 10 Hz. Participating modes are mode 1 (first wing bending), 2 (second wing bending), and 7 (wing torsion). Fore-aft modes were excluded from the analysis. This analysis provides the initial guess of the flutter dynamic pressure at $Q_f = 15485\ Pa$.

Considering that three modes are participating in the flutter, a minimum order of $p = 6$ is required for the AR part of the ARX estimation process. Allowing for aerodynamic lags, an AR order of $p = 8$ was used. The MA portion of the model was set to $q = 9$. Higher orders of the MA part did not improve the estimation results.

ARX models were estimated for the aeroelastic system in three dynamic pressure values of $0.81Q_f$, 0.87_f and $0.91Q_f$. The excitation signal was a randomly distributed vertical velocity, filtered above 120 Hz, with an amplitude of 3° angle of attack. The simulation time step was $dt = 10^-4\ s$ ($f_{Nyq} = 5000$). Since this case involves modes of higher frequency (the frequency of the torsion mode, involved in the flutter mechanism, is 22.5 Hz), this small time step was required in order to have sufficient time steps within a cycle (about 450 for the torsion mode). Responses were computed over $N = 10000$ time steps, resulting in frequency resolution of 0.5 Hz.

Figure 17 shows the roots of the characteristic equation over the unit circle of the identified system. There are three complex roots for the three participating modes (two shown in the zoom insert, one of which is very close to the real axis), and two real roots for the aerodynamic legs.

Figure 18 shows the stability parameter estimation. A linear trend line predicts flutter at $1.033Q_f$. This was verified in a full aeroelastic simulation, as shown in Figure 19.

4 SUMMARY

The paper presented a computational methodology for CFD-based flutter analysis that is based on system identification of the aeroelastic system at few sub-critical dynamic pressures, and computation of a linear stability parameter that, by extrapolation, points to the flutter conditions.

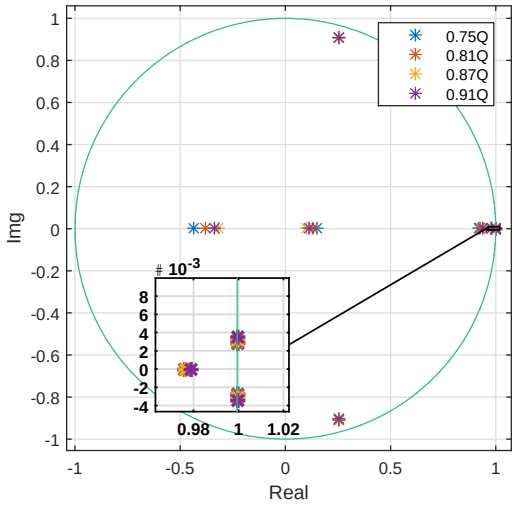

Figure 17: Roots of ARX model, $p = 8$, $q = 9$, Generic Transport Aircraft

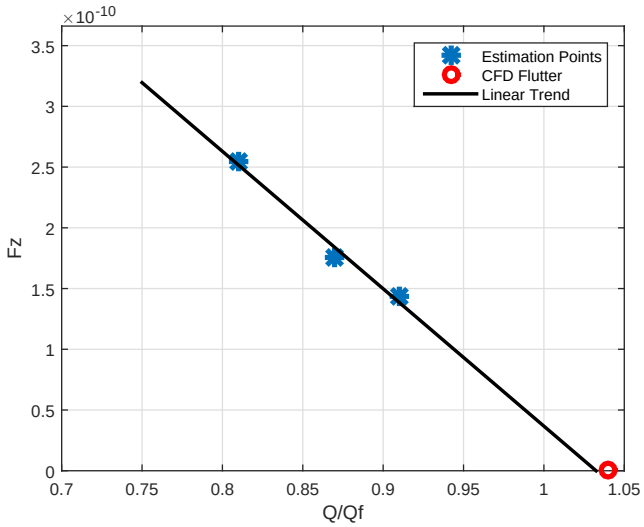

Figure 18: Stability parameter of the Generic Transport Aircraft, $p = 8$, $q = 9$

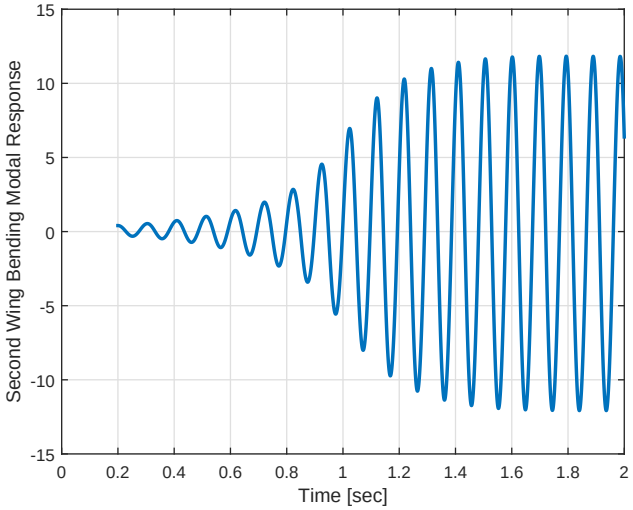

Figure 19: Time response of second mode at flutter ($1.04Q_f$), Mach=0.53, Generic Transport Aircraft

The method was demonstrated on three test cases of subsonic airfoil flutter (2 DOF plunge and pitch aeroelastic system), transonic airfoil flutter (2 DOF plunge and pitch aeroelastic system), and a generic transport aircraft at subsonic flow, with flutter mechanism involving three structural modes. In all cases the method resulted in accurate predication of the flutter point as compared to either full CFD aeroelastic simulation, or wind tunnel test results.

The method is based on simulated CFD responses to prescribed excitations, at few dynamic pressure values that are selected based on an initial guess of the flutter point, obtained from linear analysis. Responses need to be computed at two to three dynamic pressure values to generate a linear trend line of the stability parameter. At each dynamic pressure value only a single aeroelastic simulation needs to be performed, for a few thousand time steps (depending on the problem parameters). Compared to a full aeroelastic simulation that only predicts the system's stability at a single dynamic pressure value, or to methods that involve reduced-order modeling of the unsteady aerodynamic forces, and require several simulations of responses to modal excitation of each mode, the current method is highly computationally efficient.

The shortcomings of the method are that the order of the ARX model, and required length of training data, cannot be a-priori determined, and require some experimenting with. While the AR order is proportional to the number of modes participating in flutter problem, the MA order needs to be tuned for convergence of the stability parameter estimation results. Since flutter prediction is more accurate when based on stability parameter values computed close to the flutter point, some cases might require additional simulations, for generating extra data sets, in cases in which the initial guess of the flutter point is far from the real flutter point.

5 REFERENCES

[1] Geuzaine, P., Brown, G., Harris, C., et al. (2003). Aeroelastic dynamic analysis of a full f-16 configuration for various flight conditions. *AIAA Journal*, 41(3), 363–371.

[2] Melville, R. (2002). Nonlinear mechanisms of aeroelastic instability for the f-16. In *40th AIAA Aerospace Sciences Meeting*. Reston, VA: AIAA. AIAA-2002-871.

[3] Balajewicz, M. and Dowell, E. H. (2012). Reduced-order modeling of flutter and limit-cycle oscillations using the sparse volterra series. *Journal of Aircraft*, 49(6), 1803–1812.

[4] Thomas, J. P., Dowell, E. H., and Hall, K. C. (2003). Three-dimensional transonic aeroelasticity using proper orthogonal decomposition-based reduced-order models. *Journal of Aircraft*, 40(3), 544–551.

[5] Lucia, D. J., Beran, P. S., and Silva, W. A. (2005). Aeroelastic system development using proper orthogonal decomposition and volterra theory. *Journal of Aircraft*, 42(2), 509–518.

[6] Raveh, D. E. (2004). Identification of computational-fluid-dynamics based unsteady aerodynamic models for aeroelastic analysis. *Journal of Aircraft*, 41(3), 620–632.

[7] Zimmerman, N. H. and Weissenburger, J. T. (1964). Prediction of flutter onset speed based on flight testing at subcritical speeds. *Journal of Aircraft*, 1(4), 190–202.

[8] Brignac, W. J., Ness, H. B., and Smith, L. M. (1975). The random decrement technique applied to the yf-16 flight flutter tests. In *AIAA 16th Structures, Structural Dynamics and Materials Conference*. Reston, VA: AIAA. AIAA-1975-776.

[9] Matsuzaki, Y. and Ando, Y. (1981). Estimation of flutter boundary from random responses due to turbulence at subcritical speeds. *Journal of Aircraft*, 18(10), 862–868.

[10] Nissim, E. and Gilyard, G. B. (1989). Method for experimental determination of flutter speed by parameter identification. Tech. rep., NASA. TR-2923.

[11] Guillaume, P. and R. Pintelon, J. S. (1990). Description of a parametric mle in the frequency domain for mimo systems and its application to flight flutter analysis. *Mechanical Systems and Signal Processing*, 4(5), 405–416.

[12] Cooper, J. E., Emmett, P. R., Wright, J. R., et al. (1993). Envelope function: A tool for analyzing flutter data. *Journal of Aircraft*, 30(5), 785–790.

[13] Cooper, J. E. (1995). Parameter estimation methods for flight flutter testing. Tech. rep., AGARD. CP-566.

[14] Lind, R. and Brenner, M. (2000). Flutterometer: An on-line tool to predict robust flutter margins. *Journal of Aircraft*, 37(6), 1105–1112.

[15] Price, S. and Lee, B. (1993). Evaluation and extension of the flutter-margin method for flight flutter prediction. *IEEE Transactionson Circuit Theory*, 30(3), 395–402.

[16] Torii, H. and Matsuzaki, Y. (1997). Flutter boundary prediction based on nonstationary data measurement. *Journal of Aircraft*, 34(3), 427–432.

[17] Bae, J.-S., Kim, J.-Y., Lee, I., et al. (2005). Extension of flutter prediction parameter for multimode flutter systems. *Journal of Aircraft*, 42(1), 285–288.

[18] Torii, H. and Matsuzaki, Y. (2001). Flutter margin evaluation for discrete-time systems. *Journal of Aircraft*, 38(1), 42–47.

[19] Gupta, K. K. and Bach, C. (2007). Systems identification approach for a computational-fluid-dynamics-based aeroelastic analysis. *AIAA journal*, 45(12), 2820–2827.

[20] Raveh, D. E., Yossef, Y. M., and Levy, Y. (2017). Analyses for the second aeroelastic prediction workshop using the eznss code. *Submitted for publication in the AIAA journal*.

[21] Jury, I. E. (1964). *Theory and Application of the z-Transform Method*. New York: Wiley.

[22] Jury, I. and Pavlidis, T. (1963). Stability and aperiodicity constraints for system design. *IEEE Transactionson Circuit Theory*, 10(1), 137–141.

[23] Zaide, A. and Raveh, D. E. (2006). Numerical simulation and reduced-order modeling of airfoil gust response. *AIAA journal*, 44(8), 1826–1834.

[24] Matsuzaki, Y. and Torii, H. (1990). Response characteristics of a two-dimensional wing subjected to turbulence near the flutter boundary. *Journal Of Sound and Vibration*, 136(2), 187–199.

[25] B., D., M., D., R., B., et al. (1993). Experimental unsteady pressures at flutter on the supercritical wing benchmark model. In *34th AIAA/ASME/ASCE/AHS/ASC Structures, Structural Dynamics, and Materials Conference*. AIAA 93-1592.

[26] Heeg, J., Chwalowski, P., Raveh, D. E., et al. (2015). Plans and example results for the 2nd aiaa aeroelastic prediction workshop. In *56th AIAA/ASME/ASCE/AHS/ASC Structures, Structural Dynamics, and Materials Conference*. AIAA 2015-0437.

[27] Raveh, D. E. (2011). Gust-response analysis of free elastic aircraft in the transonic flight regime. *Journal of Aircraft*, 48(4), 1204–1211.

COPYRIGHT STATEMENT